A supramolecular basis for CD45 tyrosine phosphatase regulation in sustained T cell activation

Kenneth G. Johnson*†, Shannon K. Bromley†, Michael L. Dustin†‡, and Matthew L. Thomas*†

*Howard Hughes Medical Institute and †Department of Pathology and Immunology, Washington University School of Medicine, St Louis MO 63110

Communicated by Emil R. Unanue, Washington University School of Medicine, St. Louis, MO, June 28, 2000 (received for review March 20, 2000)

Transmembrane protein tyrosine phosphatases, such as CD45, can act as both positive and negative regulators of cellular signaling. CD45 positively modulates T cell receptor (TCR) signaling by constitutively priming p56lck through the dephosphorylation of the C-terminal negative regulatory phosphotyrosine site. However, CD45 can also exert negative effects on cellular processes, including events triggered by integrin-mediated adhesion. To better understand these opposing actions of tyrosine phosphatases, the subcellular compartmentalization of CD45 was imaged by using laser scanning confocal microscopy during functional TCR signaling of live T lymphocytes. On antigen engagement, CD45 was first excluded from the central region of the interface between the T cell and the antigen-presenting surface where CD45 would inhibit integrin activation. Subsequently, CD45 was recruited back to the center of the contact to an area adjacent to the site of sustained TCR engagement. Thus, CD45 is well positioned within a supramolecular assembly in the vicinity of the engaged TCR, where CD45 would be able to maintain src-kinase activity for the duration of TCR engagement.

Transmembrane protein tyrosine phosphatases can exert both positive and negative effects on cell signaling (1, 2). The transmembrane protein tyrosine phosphatase CD45 is critical for activation through the T cell receptor (TCR) after recognition of agonist peptide presented by the appropriate MHC molecule (3). CD45 positively regulates T cell activation through the dephosphorylation of the negative regulatory C-terminal tyrosine phosphorylation sites of the src-kinase molecules p56lck and p59fyn (4–8). However, CD45 has a broad substrate specificity and can also act as a negative regulator of cell signaling (2, 5). Specifically, CD45 has been shown to negatively regulate the autocatalytic tyrosine phosphorylation site of src-kinase molecules and has the ability to dephosphorylate components of the TCR complex (9–13). The cellular consequences of tyrosine phosphatase activity may be determined, in part, by the specific compartmentalization of tyrosine phosphatases with respect to cell-surface receptors (2, 14–17). Sustained engagement of the TCR results in the large-scale receptor compartmentalization of multiple supramolecular activation clusters at a specialized interface between the T cell and the antigen-presenting cell termed the immunological synapse (18–23). Importantly, the formation of the immunological synapse on live T cells can be imaged with diffraction-limited resolution on planar lipid bilayers containing fluorescently labeled glycosylphosphatidylinositol (GPI)-linked forms of I-E^k-presenting agonist peptide and intracellular adhesion molecule 1 (ICAM-1) (19). The immunological synapse offers a unique opportunity to examine tyrosine phosphatase compartmentalization in relation to well defined physiological supramolecular activation clusters and was used in conjunction with confocal fluorescence microscopy to study the distribution of CD45 on live T cells during functional ligand engagement of the TCR.

Materials and Methods

Constructs and Planar Bilayers. GPI-E^k and GPI-ICAM-1 expressed in Chinese hamster ovary (CHO) and BHK cells were purified, labeled with Oregon green (Molecular Probes) and Cy5 (Amersham Pharmacia), respectively, and reconstituted into phosphatidylcholine (egg) vesicles as described (19). GPI-E^k and GPI-ICAM-1 liposomes were mixed 1:1, incubated on clean glass in a parallel-plate flow cell (Bioptechs, Butler, PA) (24), and pulsed with 50 μM peptide for 4 h at 37°C.

Cells. Splenocytes from 2B4 TCR α-chain knock-in mice expressing the clonotypic 2B4 TCR (25) were cultured with 1 μM agonist peptide [moth cytochrome *c* (MCC) 91–103] for 3 days in RPMI medium 1640 supplemented with FCS, glutamine, penicillin, streptomycin, and 2-mercaptoethanol. Cells were then expanded with 100 units/ml of IL-2 and used on days 5–7. Cells were labeled for 15 min at room temperature in Hanks' balanced salt solution (HBSS) containing 1% human serum albumin, with Alexa546-conjugated I3/2.3 Fab fragments, or with Cy5-conjugated I3/2.3 Fab fragments and Alexa546-conjugated H57 Fab fragments. Molecular densities of CD45 and TCR on 2B4 T lymphocytes were calculated as 2,500 molecules/μm^2 and 150 molecules/μm^2, respectively, by cold-competition immunoradiometric assays.

Confocal Imaging. Digitized three-color fluorescence images were obtained with an inverted Plan Apochromat ×63/1.4 oil objective on a Zeiss LSM 510 Confocal Microscope, with emission spectra defined by broad pass (505–550 nm, 560–615 nm) and long pass (650 nm) filters, and uniform pinholes (160 μm). Sections (1.0 μm thick) were imaged to a resolution of ≈200 nm in the xy plane. For controls, labeled 2B4 T cells were allowed to settle on bilayers containing ICAM-1, or on glass coated with poly-L-lysine. Receptor densities are referenced to this baseline, which was identical on the two control substrates. After background subtraction and photobleaching adjustment, receptor density accumulation was determined as follows: accumulation (molecules/μm^2) = receptor density (molecules/μm^2)−baseline density (molecules/μm^2), where receptor density (molecules/μm^2) = [fluorescence intensity (units/μm^2)/baseline fluorescence intensity (units/μm^2)] × baseline density (molecules/μm^2). For colocalization analysis, 3 × 8-bit RGB fluorescence channels were split and individually thresholded at a minimum of 150 pixel intensity units (≈60%). A colocalization algorithm was applied between paired channels to assess the position and number of aligned positive (white) pixels, where colocalization (%) = number of aligned pixels (between 2 channels)/number of positive pixels (for 1 channel). Colocalization was assessed in a defined region of the immunological synapse, eliminating the

Abbreviations: TCR, T cell receptor; ICAM-1, intracellular adhesion molecule 1; LFA-1, lymphocyte function-associated antigen 1; GPI, glycosylphosphatidylinositol.

‡To whom correspondence should be addressed at: Department of Pathology, Washington University Medical School, Campus Box 8118, 660 South Euclid Street, St. Louis, MO 63110. E-mail: dustin@immunology.wustl.edu.

The publication costs of this article were defrayed in part by page charge payment. This article must therefore be hereby marked "*advertisement*" in accordance with 18 U.S.C. §1734 solely to indicate this fact.

bright outer ring of high CD45 fluorescence intensity. For photobleaching, a 1-μm diameter spot was exposed to a pulse of 100% laser intensity at 488 nm and 620 nm to produce an irreversible photobleaching of the fluorochromes. The recovery process is a function of both the kinetic rates for the receptor ligand interaction and the density and diffusion or active movement of free molecules within the bilayer and on the cell surface (26).

Results and Discussion

CD45 Is Recruited to the Center of the Immunological Synpase. CD45 on cultured T cells from 2B4 TCR transgenic mice was labeled with fluorochrome-conjugated Fab fragments from the I3/2.3 monoclonal antibody, which recognizes all CD45 isoforms (27). Fluorescent intensities were calibrated to molecular densities by radioimmunometric assay and imaging on poly-L-lysine control substrates that did not induce molecular redistribution. Labeled T cells were settled onto prewarmed (37°C) planar lipid bilayers presenting the 91–103 peptide from moth cytochrome *c* (MCC 91–103) in the context of fluorescently labeled GPI-anchored forms of I-E^k (MHC-peptide) and ICAM-1 molecules, as described (19). Areas of tight apposition between the T cell and the planar bilayer were defined by interference reflection microscopy (IRM) (28), and confocal laser scanning microscopy was used to acquire fluorescence images. Approximately 30% of T cells formed mature immunological synapses in response to the activating antigen within 30 min of settling on the planar bilayer, as defined by a $\approx$5-μm diameter ring of ICAM-1 accumulation (red) surrounding a central accumulation of MHC-peptide complexes (green) (Fig. 1 *A* and *B*). The ICAM-1 ring was surrounded by an outer ring of high CD45 density that may be accounted for by imaging two layers of closely apposed T cell membrane. More importantly, high intensity staining of CD45 was observed inside the ICAM-1 ring, within the vicinity of the clustered MHC-peptide, in over 90% of cells that formed the mature immunological synapse (Fig. 1*A*; arrows indicate cells accumulating CD45 within the immunological synapse). The yellow arrow in Fig. 1*B* indicates recruitment of CD45 to the vicinity of the clustered MHC-peptide. In addition, CD45 staining was notably decreased within regions of lymphocyte function-associated antigen 1 (LFA-1)/ICAM-1 engagement in a manner that was entirely antigen dependent (Fig. 1 *B* and *C*). Confocal imaging reveals why previous studies have failed to detect the specific compartmentalization of CD45 within the central region of the immunological synapse, which may be obscured by the bright outer ring of CD45 with conventional fluorescence imaging techniques (29).

Dynamic Compartmentalization of CD45 Within the Developing Immunological Synapse. To directly assess the location of CD45 with respect to the TCR, T cells were stained with fluorescently labeled Fab fragments of I3/2.3 and the nonblocking β-chain-specific monoclonal antibody, H57 (30). Importantly, Fab fragments of I3/2.3 and H57 did not prevent cellular proliferation in response to antigen presented by the planar bilayers. H57 Fab fragments did show a slight inhibition of T cell proliferation at saturating doses, but proliferation was still 80% of that recorded for unlabeled cells (see Fig. 6, which is published as supplemental data on the PNAS web site, www.pnas.org). T cells recognizing ICAM-1 and activating MHC-peptide complexes within planar lipid bilayers stop migrating and cluster ICAM-1 molecules within 30 seconds. ICAM-1 then moves away from the center of the contact, simultaneously with the central accumulation of MHC-peptide complexes (19, 21). The dynamics of CD45 accumulation within the immunological synapse demonstrated biphasic kinetics similar to these previously defined processes (Figs. 2 and 3, and Movies 1–4 in the supplemental data). The formation of the mature immunological synapse is illustrated in

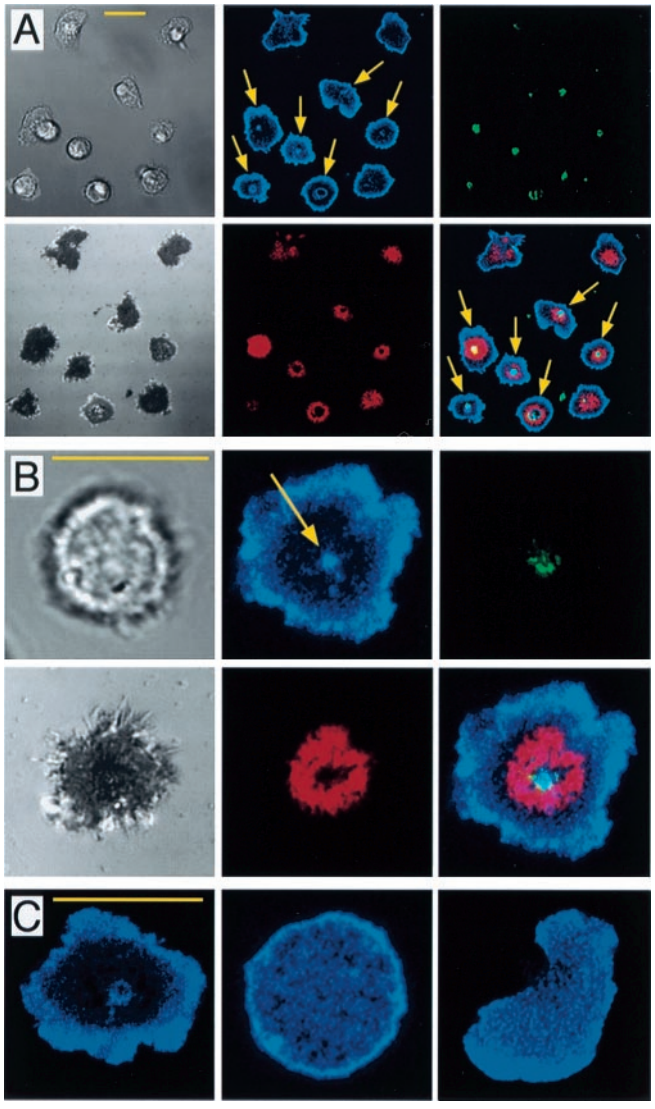

Fig. 1. Localization of CD45 to the central region of the mature immunological synapse. I3/2.3-Alexa546-labeled T cells were settled onto lipid bilayers containing Cy-5-conjugated ICAM-1, and Oregon green-conjugated agonist MHC-peptide. ICAM-1 (red), MHC-peptide (green), CD45 (blue). (Scale bars = 10 μm.) (*A* and *B*) Interference reflection microscopy and fluorescent images of the T cell/bilayer interface. (*Upper Left*) Transmitted light. (*Lower Left*) Interference reflection microscopy. (*Lower Right*) Red/green/blue overlay. $n = 300$. (*C*) Fluorescent images of CD45 density at the cell/bilayer interface. (*Left*) Peptide/MHC/ICAM substrate. (*Middle*) Poly-L-lysine substrate. (*Right*) ICAM-1 substrate.

Fig. 2*A*, demonstrating the movement of MHC-peptide (green), TCR (red), and CD45 (blue). Fig. 2*B* displays TCR/CD45 movement as red/green overlays during the formation of the immunological synapse on three representative cells. Initially, both TCR and CD45 were uniformly distributed on the surface of the T cells (data not shown). On contact with the antigen-containing bilayer and the termination of cell migration, CD45 first moved away from the center of the contact corresponding to the area of ICAM-1 accumulation within 3.5 min of settling, as noted by the decrease in blue intensity in the center of the contact region (Fig. 2*A*). Quantitatively, this loss of CD45 from the bilayer contact area amounted to a decrease of 1,500 molecules/μm^2 within this early time period (Fig. 3*A*). In nine individual experiments, this change of CD45 density ranged between decreases of 750 to 2,000 molecules/μm^2. Within the

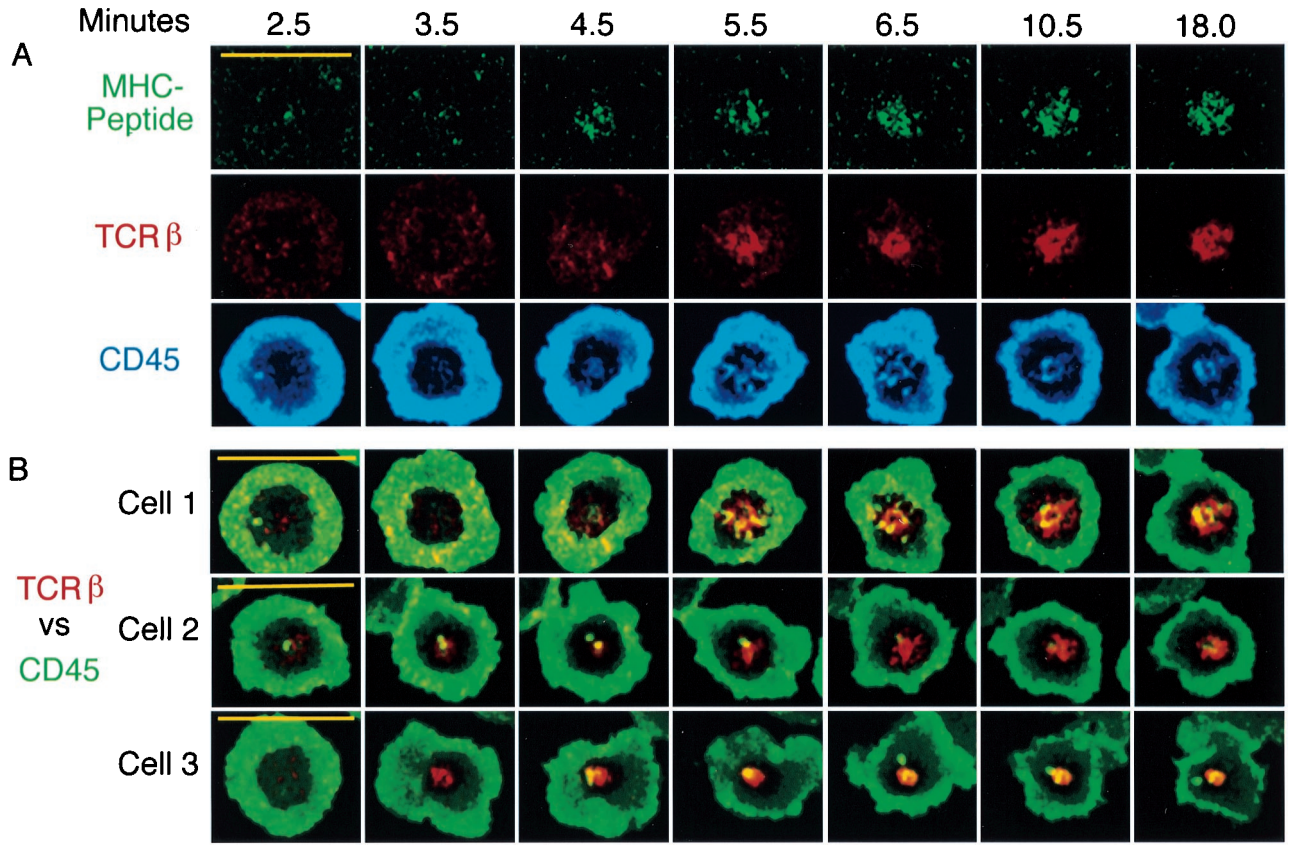

Fig. 2. Dynamics of CD45 distribution during the formation of the immunological synapse. T cells were labeled with I3/2.3-Cy5 and H57-Alexa546 and settled onto bilayers incorporating unlabeled ICAM-1, and Oregon green-conjugated MHC-peptide. (Scale bars = 10 μm.) (*A*) Synapse formation at the T cell/bilayer interface. TCR (red), MHC-peptide (green), CD45 (blue). (*B*) Red/green overlays of TCR and CD45 distribution during the formation of the immunological synapse on three representative cells. TCR (red), CD45 (green).

subsequent 10 min after this redistribution, CD45 was clustered into the center of the cell/bilayer contact (Fig. 2*A*) and returned to a density greater than the initial basal value of 2,500 sites/μm^2 in all cells examined (Fig. 3*A*). In parallel with this redistribution of CD45, the TCR on the T cell and MHC-peptide on the planar bilayer demonstrated the specific accumulation of 700 molecules/μm^2 and 400 molecules/μm^2, respectively, at the center of the cell/bilayer contact area (Fig. 3). In all experiments, the accumulation of TCR was always observed to be 2- to 3-fold higher than MHC-peptide recruitment. CD45 displayed a degree of colocalization with TCR during the accumulation of CD45 to the center of the contact area, but CD45 was also capable of entering the synapse in pools distinct from the TCR, being recruited as discrete aggregates from the peripheral ring of high membrane area. Red/green overlays of TCR/CD45 fluorescence (Fig. 2*B*, and Movies 1–4 in the supplemental data) show regions of colocalization but also some regions of segregation of TCR from CD45. In Fig. 2*B*, Cell 1, regions of colocalization of TCR and CD45 can be seen (5.5 min, red/green = yellow), but a degree of segregation is also apparent at other time points (6.5 min). Pixel alignment analyses revealed a high level of colocalization of TCR with MHC-peptide in the developing immunological synapse (up to 10 min), but a lower level of colocalization of TCR with CD45 during this period (Fig. 3*B*). MHC-peptide displayed 70% colocalization with TCR within 5 min of cells contacting the bilayer, whereas, at this same point in time, only 29% of CD45 in the developing immunological synapse was colocalized with TCR. By 11 min, TCR colocalization with CD45 had increased to 70%, but by 40 min this colocalization returned to below 30%. In contrast, MHC-peptide consistently main-

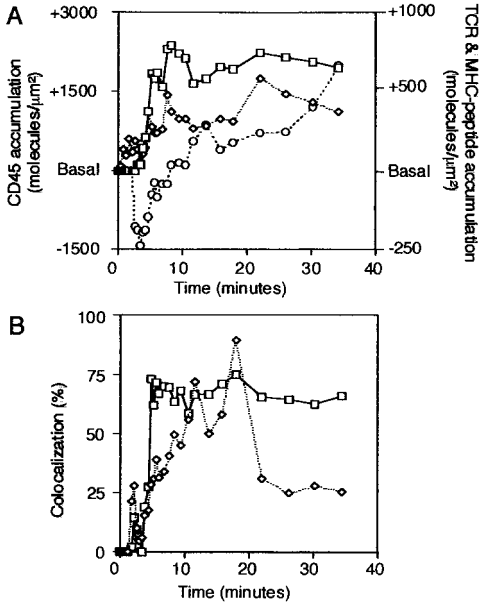

Fig. 3. Kinetics of CD45 distribution during the formation of the immunological synapse. Data are representative of nine cells. Data shown are for Cell 1, Fig. 2*B*. (*A*) Density accumulation (molecules/μm^2) was assessed for CD45 (open circles) and TCR (open squares) on the T cell, and MHC-peptide (open diamonds) within the planar bilayer. (*B*) Analysis of MHC-peptide positive pixels colocalized with TCR (open squares) and CD45 positive pixels colocalized with TCR (open diamonds) during the formation of the immunological synapse.

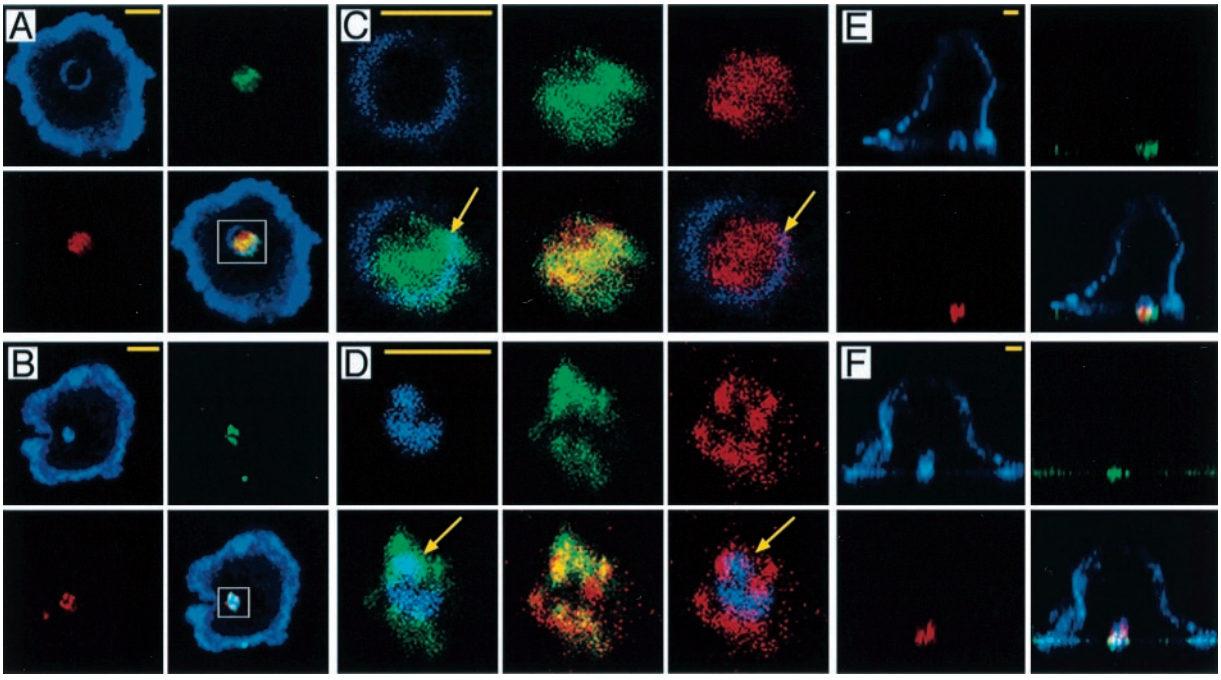

Fig. 4. Segregation of CD45 and engaged TCR in the central region of the immunological synapse. T cells were labeled with I3/2.3-Cy5, and H57-Alexa546 Fab fragments and settled onto planar lipid bilayers incorporating unlabeled ICAM-1, and Oregon green-conjugated agonist MHC-peptide. TCR (red), MHC-peptide (green), CD45 (blue). Data are representative of 50 individual cells. (Scale bars = 1 μm.) (*A* and *B*) Fluorescent images at the cell/bilayer interface. (*Lower Right*) Red/green/blue overlay. Boxes show the area examined in greater detail in *C* and *D*. (*C* and *D*) High detail (850 data points/μm^2) profiling of the immunological synapse. (*Upper*, left to right) CD45 (blue), MHC-peptide (green), and TCRβ (red). (*Lower*, left to right) Overlays of CD45/MHC-peptide(blue/green), MHC-peptide/TCR(green/red), and CD45/TCR (blue/red). (*E* and *F*) Confocal z-stacks are sectioned through the x-plane and presented with the z-plane on the vertical axis. (*Lower Right*) Red/green/blue overlay.

tained 70% colocalization with the TCR for the duration of the experiment. In multiple experiments, TCR consistently displayed a higher degree of colocalization with the MHC-peptide than with CD45 throughout the time course. Thus CD45, unlike MHC-peptide, can be transported independently of the TCR within the immunological synapse.

The recruitment of TCR and CD45 to the immunological synapse was highly reproducible on all cells examined, although the kinetics of these processes did vary slightly between individual cells. In Fig. 2*B*, Cell 2, the movement of CD45 to the immunological synapse occurred rapidly, being simultaneous with the loss of CD45 from the region of (unlabeled) ICAM-1 engagement and appeared as a single discrete pool of CD45 that was independent of TCR (2.5 to 3.5 min). In this case, TCR movement was slightly delayed and was maximal at 6.5 min. Conversely, in Fig. 2*B*, Cell 3, accumulation of TCR was rapid (by 3.5 min), and CD45 recruited slightly later (at 4.5 min) to the vicinity of the TCR from the left hand side of the cell. Some pools of CD45 were extremely mobile within the immunological synapse, whereas others were not. Notably, in Fig. 2, Cells 2 and 3 (and supplemental Movies 2–4), pools of CD45 moved rapidly in and out of the central region of the immunological synapse independent of the TCR. These pools were capable of crossing the LFA-1 ring (supplemental Movie 5). It is possible that a continuous shuttling mechanism involving CD45 may contribute to sustained T cell signaling within the immunological synapse. The rapid cell surface labeling procedure used with Fab fragments suggests that the CD45 imaged was expressed on the cell surface, the movement of which may perhaps be regulated by specific membrane microenvironments and/or cytoskeletal components. However, it is also possible that pools of CD45 could be internalized in activated cells and translocated through submembranous vesicular structures.

TCR Segregation from CD45 in the Immunological Synpase. To examine the spatial relationship of CD45 and the TCR further, the localization of CD45 in relation to the TCR was assessed on numerous T cell/antigen conjugates displaying the mature immunological synapse. TCR (red) clustered within the central region of the immunological synapse overlapped extensively with areas of MHC-peptide accumulation (green) (Fig. 4 *A* and *B*). CD45 (blue) was observed to be in close proximity to both TCR and MHC-peptide clusters within the immunological synapse (Fig. 4 *A* and *B*). High detail analysis (85$\varnothing$ data points/μm^2) of the central region of the immunological synapse demonstrated that much of the clustered TCR was colocalized with the accumulated MHC-peptide complexes (red/green overlay = yellow), although fractions of clustered TCR and MHC-peptide were spatially distinct (Fig. 4 *C* and *D*). Whereas some TCR was colocalized with CD45 (Fig. 4*C*, yellow arrows), a large proportion of the TCR was segregated away from regions of high CD45 staining, with CD45 either found as symmetric or asymmetric bodies surrounding the TCR/MHC-peptide cluster (Fig. 4*C*) or, alternatively, located in pockets of low density TCR/MHC-peptide staining within the accumulated TCR/MHC-peptide clusters (Fig. 4*D*). Quantitative analysis of binary images demonstrated that >60% of the TCR was colocalized with MHC-peptide, but only 30% was associated with CD45, suggesting that a large proportion of the accumulated TCR was segregated away from CD45 at any given time (see supplemental Fig. 7). However, TCR was always positioned within 0.5 μm of high density CD45 accumulation (Fig. 2 *C* and *D*). The dynamics of these distributions may prove to be important for maintaining a sustained T cell signal. In addition, there is evidence to suggest a more 3-dimensional aspect to the interplay of CD45 with the TCR (Fig. 4 *E* and *F*). Accumulated CD45 projected into the cell to define a novel supramolecular structure, often noted to be

dome-like, above the TCR and the plane of the bilayer (Fig. 4*E* and supplemental Movie 5). In a two-dimensional aspect, this dome-like structure translates as a ring-structure at the cell/bilayer interface (Fig. 1 *A* and *C* and Fig. 4*A*). This phenomena was not an artifact of confocal imaging, as judged by fluorochrome-swapping, and analytical imaging of tri-fluorescent beads. There was some heterogeneity to the precise form of this structure, because the inward projection was also seen without a dome-like character (Fig. 4*F*). High-resolution ultrastructural studies will be required to resolve these issues in greater detail. The current fluorescence studies strongly suggest both temporal and three-dimensional aspects for the interplay between the TCR and CD45 within the immunological synapse.

Dynamic Exchange of CD45 Within the Mature Immunological Synapse. TCR-engaged MHC-peptide complexes within the mature immunological synapse are isolated from free MHC-peptide complexes in the bilayer, as demonstrated by fluorescence photobleaching recovery experiments (19). To assess CD45 mobility, the central region of the mature immunological synapse was bleached to irreversibly eliminate fluorescence without damage to the molecular structures, and the fluorescence recovery was assessed over time. MHC-peptide clusters at the center of the immunological synapse were unable to recover any significant fluorescence, even up to 45 min after bleaching, as previously described (Fig. 5 *A* and *B*) (19). CD45 at the periphery of the cell/bilayer contact, represented by the bright outer ring of CD45 staining, demonstrated complete fluorescence recovery within 30 sec after photobleaching (Fig. 5 *A* and *B*). Large fluctuations observed for the fluorescence intensity of this peripheral CD45 was due to the dynamic "ruffling" nature of the membrane in this region. Interestingly, CD45 clustered within the central region of the immunological synapse also demonstrated photobleaching recovery, although this recovery was slower and incomplete as compared with the photobleaching recovery of the peripheral pool of CD45 outside the immunological synapse. Accumulated CD45 demonstrated 15% recovery of fluorescence intensity within 30 seconds and never exceeded 60% recovery of the original fluorescence intensity within the 45-min time course. Therefore, centrally accumulated CD45 is able to exchange with the larger pool of freely diffusing CD45 outside the immunological synapse although its mobility is significantly restricted. This phenomenon may reflect the movement of punctate pools of accumulated CD45 across the ICAM-1 ring (Fig. 2*B*, supplemental Movies 2–4), allowing limited exchange of components in and out of the immunological synapse.

A Supramolecular Basis for the Opposing Roles of CD45 in T Lymphocyte Regulation. This study reveals the dynamic nature of tyrosine phosphatase compartmentalization after ligand engagement of a cell surface receptor. The initial decrease of CD45 density on TCR engagement correlates with the formation of LFA-1/ICAM-1 interactions and may in fact be important for LFA-1 activation, based on the demonstrated ability of CD45 to inhibit integrin function (9, 10). This finding is consistent with recent studies that demonstrate CD45 exclusion from the synapse at early time points (31). CD45 constitutively dephosphorylates the C-terminal phosphorylation site of p56lck, maintaining p56lck in a "primed" active state to enable rapid signaling on antigen engagement of the TCR (32). However, it has been shown that TCR-mediated calcium signaling can be terminated within seconds of CD45 phosphatase inactivation through the dimerization of chimeric CD45 molecules, suggesting that CD45 phosphatase activity is continuously required throughout antigen engagement (33). The tyrosine kinase csk phosphorylates the C-terminal negative regulatory site of src-family kinases and thus antagonizes the action of CD45 (5). Csk is cytosolic but can be recruited

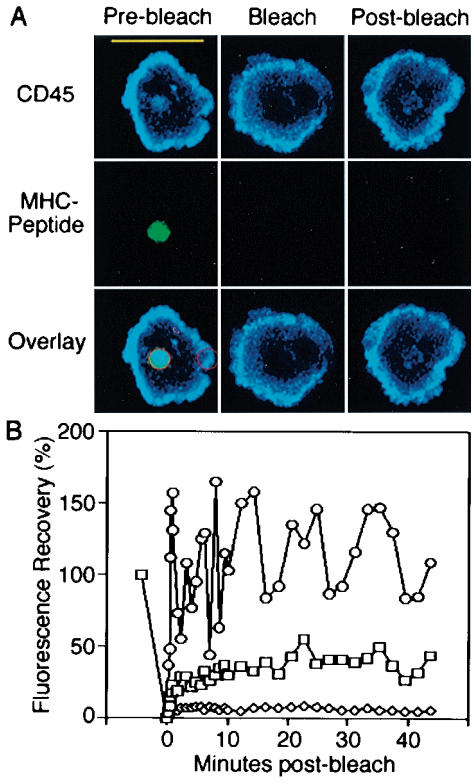

Fig. 5. Photobleaching recovery of CD45 within the immunological synapse. (*A*) T cells labeled with I3/2.3-Cy5 Fab fragments were allowed to form the mature immunological synapse on planar bilayers containing unlabeled ICAM-1 and Oregon green-conjugated MHC-peptide. Fluorescence from accumulated MHC-peptide (green) and CD45 (blue) was quenched by photobleaching at the position shown (red circles). (Scale bar = 10 μm.) (*B*) Bleaching recovery kinetics are represented as the percentage recovery of fluorescence after photobleaching for CD45 (open squares) and MHC-peptide (open diamonds) within the immunological synapse, and also for CD45 at the periphery of the cell/bilayer contact region (open circles). Data are representative of five individual experiments.

to the plasma membrane through the binding of its src homology 2 (SH-2) domain to a tyrosine phosphorylated transmembrane protein, PAG/cbp (34, 35). The compartmentalization of PAG/cbp within detergent insoluble lipid microdomains may locate csk adjacent to its src-kinase substrates (34, 35). Interestingly, PAG is constitutively tyrosine phosphorylated in resting T cells and is rapidly dephosphorylated after T cell activation, releasing csk (34). Although the kinetics of PAG–csk interactions within the sustained signaling environment of the immunological synapse are not known, a reciprocal recruitment of CD45 and loss of csk in the immunological synapse may act in concert to maintain src-kinase molecules in an activated state. The close proximity of CD45 to the TCR may be critical to allow primed p56lck to reach the engaged TCR before inactivation by csk. Assuming that p56lck has a diffusion coefficient similar to other lipid-anchored membrane proteins and employing the general equation for two dimensional diffusion half-time (τ = distance^2/4D, where diffusion coefficient (D) = 0.1 μm^2/s), primed p56lck molecules would diffuse from the centrally clustered CD45 to the engaged TCR within 0.5 sec (36). In contrast, p56lck would take $\approx$1 min to diffuse from the outer ring of CD45 to the engaged TCR. In addition, the dynamic relationship of CD45 and TCR in the central region of the immunological synapse may transiently allow pools of TCR to be particularly closely associated with CD45. Importantly, a degree of segregation of the TCR

from CD45 may be necessary to prevent negative regulation of proximal signaling processes. This segregation may result either from the exclusion of CD45 from specific membrane microenvironments, or from steric constraints governed by the large extracellular domain of CD45, and may also be regulated on a more temporal basis (2, 4, 15, 37, 38). A ligand for CD45 remains to be identified and would be clearly absent from the supported planar bilayers used in this study. Whereas a ligand for CD45 could be present on the surface of the T cell itself, it is perhaps more likely that the movement of CD45 to the central region of the immunological synapse operates through the intracellular or transmembrane portions of CD45, perhaps involving CD45-associated protein (CD45AP) or cytoskeletal connections (39, 40). Live cell imaging of protein compartmentalization reveals a novel facet of cellular regulation by transmembrane protein tyrosine phosphatases and, viewed alongside established biochemical and functional data, greatly adds to our understanding of the roles of transmembrane tyrosine phosphatases in the regulation of cell signaling.

This paper is dedicated to the memory of Matthew L. Thomas. We thank O. Kanagawa for 2B4 TCR α knock-in β transgenic mice. We also thank T. Woodford-Thomas, P. M. Allen, E. R. Unanue, and A. C. Chan for critical review of the manuscript. This work supported by grants from the Howard Hughes Medical Institute (M.L.T.), the Whitaker Foundation (M.L.D.), the Arthritis Foundation (M.L.D.), and the National Institutes of Health (M.L.T. and M.L.D.).

1. Den Hertog, J., Blanchetot, C., Buist, A., Overvoorde, J., Van Der Sar, A. & Tertoolen, G. J. (1999) *Int. J. Dev. Biol.* **43,** 723–733.
2. Thomas, M. L. & Brown, E. J. (1999) *Immunol. Today* **20,** 406–411.
3. Qian, D. & Weiss, A. (1997) *Curr. Opin. Cell Biol.* **9,** 205–212.
4. Thomas, M. L. (1994) *Curr. Opin. Cell Biol.* **6,** 247–252.
5. Weil, R. & Veillette, A. (1996) *Curr. Top. Microbiol. Immunol.* **205,** 63–87.
6. Kishihara, K., Penninger, J., Wallace, V. A., Kundig, T. M., Kawai, K., Wakeham, A., Timms, E., Pfeffer, K., Ohashi, P. S., Thomas, M. L., *et al*. (1993) *Cell* **74,** 143–156.
7. Byth, K. F., Conroy, L. A., Howlett, S., Smith, A. J., May, J., Alexander, D. R. & Holmes, N. (1996) *J. Exp. Med.* **183,** 1707–1718.
8. Seavitt, J. R., White, L. S., Murphy, K. M., Loh, D. Y., Perlmutter, R. M. & Thomas, M. L. (1999) *Mol. Cell. Biol.* **19,** 4200–4208.
9. Roach, T. I. A., Slater, S. E., Koval, M., White, L., Cahir McFarland, E. D., Okumura, M., Thomas, M. L. & Brown, E. J. (1997) *Curr. Biol.* **7,** 408–417.
10. Shenoi, H. D., Seavitt, J., Zheleznyak, A., Thomas, M. L. & Brown, E. J. (1999) *J. Immunol.* **162,** 7120–7127.
11. D'Oro, U. & Ashwell, J. D. (1999) *J. Immunol.* **162,** 1879–1883.
12. Furukawa, T., Itoh, M., Kreugar, N. X., Streuli, M. & Saito, H. (1994) *Proc. Natl. Acad. Sci. USA* **91,** 10928–10932.
13. Gervais, F. G. & Veillette, A. (1997) *J. Biol. Chem.* **272,** 12754–12761.
14. van der Merwe, A. P., Davis, S. J., Shaw, A. S. & Dustin, M. L. (2000) *Semin. Immunol.* **12,** 5–21.
15. Rodgers, W. & Rose, J. K. (1996) *J. Cell. Biol.* **135,** 1515–1523.
16. Leitenberg, D., Boutin, Y., Dan Lu, D. & Bottomly, K. (1999) *Immunity* **10,** 701–711.
17. Serra-Pages, C., Medley, Q. G., Tang, M., Hart, A. & Streuli, M. (1998) *J. Biol. Chem.* **273,** 15611–15620.
18. Paul, W. E. & Seder, R. A. (1994) *Cell* **76,** 241–251.
19. Grakoui, A., Bromley, S. K., Sumen, C., Davis, M. M., Shaw, A. S., Allen, P. M. & Dustin, M. L. (1999) *Science* **285,** 221–227.
20. Viola, A., Schroeder, S., Sakakibara, Y. & Lanzavecchia, A. (1999) *Science* **283,** 680–682.
21. Monks, C. R. F., Freiberg, B. A., Kupfer, H., Sciaky, N. & Kupfer, A. (1998) *Nature (London)* **395,** 82–86.
22. Wulfing, C. & Davis, M. M. (1998) *Science* **282,** 2266–2269.
23. Wülfing, C., Sjaastad, M. D. & Davis, M. M. (1998) *Proc. Natl. Acad. Sci. USA* **95,** 6302–6307.
24. McConnell, H. M., Watts, T. H., Weis, R. M. & Brian, A. A. (1986) *Biochim. Biophys. Acta* **864,** 95–106.
25. Wang, F., Huang, C.-H. & Kanagawa, O. (1998) *Proc. Natl. Acad. Sci. USA* **95,** 11834–11839.
26. Elson, E. L. & Qian, H. (1989) *Methods Cell Biol.* **30,** 307–332.
27. Trowbridge, I. S. (1978) *J. Exp. Med.* **148,** 313–323.
28. Sackmann, E. (1996) *Science* **271,** 43–48.
29. Sperling, A. I., Sedy, J. R., Manjunath, N., Kupfer, A., Ardman, B. & Burkhardt, J. K. (1998) *J. Immunol.* **161,** 6459–6462.
30. Wang, J., Lim, K., Smolyar, A., Teng, M., Liu, J., Tse, A. G., Liu, J., Hussey, R. E., Chishti, Y., Thomson, C. T., *et al*. (1998) *EMBO J.* **17,** 10–26.
31. Leupin, O., Zaru, R., Laroche, T., Muller, S. & Valitutti, S. (2000) *Curr. Biol.* **10,** 277–280.
32. Pingel, J. T., Cahir McFarland, E. D. & Thomas, M. L. (1994) *Int. Immunol.* **6,** 169–178.
33. Desai, D. M., Sap, J., Silvennoinnen, O., Schlessinger, J. & Weiss, A. (1994) *EMBO J.* **13,** 4002–4010.
34. Brdika, T., Pavlitová, D., Leo, A., Bruyns, E., Koínek, V., Angelisová, P., Scherer, J., Shevchenko, A., Shevchenko, A., Hilgert, I., *et al*. (2000) *J. Exp. Med.* **191,** 1591–1604.
35. Kawabuchi, M., Satomi, Y., Takao, T., Shimonishi, Y., Nada, S., Nagai, K., Tarakhovsky, A. & Okada, M. (2000) *Nature (London)* **404,** 999–1003.
36. Sheets, E. D., Lee, G. M., Simson, R. & Jacobson, K. (1997) *Biochemistry* **36,** 12449–12458.
37. Shaw, A. S. & Dustin, M. L. (1997) *Immunity* **6,** 361–369.
38. van der Merwe, P., McNamee, P., Davies, E., Barclay, A. & Davis, S. (1995) *Curr. Biol.* **5,** 74–84.
39. Cahir McFarland, E. D., Pingel, J. & Thomas, M. L. (1997) *Biochemistry* **36,** 7169–7175.
40. Iida, N., Lokeshwar, V. B. & Bourguignon, L. Y. (1994) *J. Biol. Chem.* **269,** 28576–28583